Three-dimensional modelling of aortic leaflet coaptation and load-bearing surfaces: *in silico* design of aortic valve neocuspidizations

Loïc Georges Macé [a,b,*], Tom Fringand[b], Isabelle Cheylan[b], Laurent Sabatier[c], Laurent Meille[d], Marien Lenoir[a,b] and Julien Favier[b]

[a]Department of Cardiac Surgery, La Timone Hospital, AP-HM, Aix Marseille Univ, Marseille, France
[b]Aix Marseille Univ, CNRS, Centrale Med, M2P2, Marseille, France
[c]Aix Marseille Univ, CNRS, Centrale Med, LMA, Marseille, France
[d]Cardiovascular Department, Clinique Rhône Durance, Avignon, France

* Corresponding author. Département de Chirurgie Cardiaque, Hôpital de la Timone, AP-HM, Aix Marseille Univ, 264 Rue Saint Pierre, 13385 Marseille, France. Tel: +33-491-386-496; fax: + 33-491-384-576; e-mail: loic.mace@ap-hm.fr (L.G. Macé).

Three-dimensional modelling of aortic leaflet coaptation and load-bearing surfaces: In silico design of aortic valve neocuspidizations

Summary

Geometric Morphometrics, using landmarks along the geometric determinants of the aortic valve, from computed tomography, combined with three-dimensional (3D) Non-Uniform Rational Basis Splines (NURBS), reliably defines the modelling of the coaptation and load-bearing surfaces of the aortic valve and could be used to design aortic valve neocuspidization on a case-by-case basis.

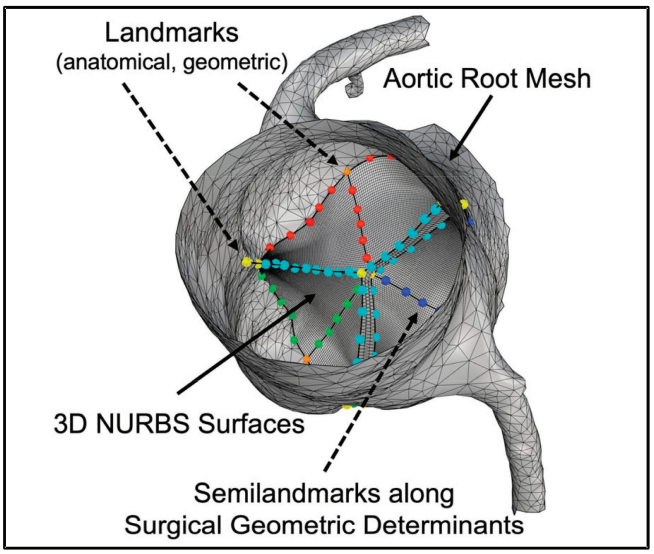

Legend: Individualized modelling of the aortic valve. 3D, three-dimensional; NURBS, Non-Uniform Rational Basis Splines.

Abstract

OBJECTIVES: Three-dimensional (3D) modelling of aortic leaflets remains difficult due to insufficient resolution of medical imaging. We aimed to model the coaptation and load-bearing surfaces of the aortic leaflets and adapt this workflow to aid in the design of aortic valve neocuspidizations.

METHODS: Geometric morphometrics, using landmarks and semilandmarks, was applied to the geometric determinants of the aortic leaflets from computed tomography, followed by an isogeometric analysis using Non-Uniform Rational Basis Splines (NURBS). Ten aortic

valve models were generated, measuring determinants of leaflet geometry defined as 3D NURBS curves, and leaflet coaptation and load-bearing surfaces were defined as 3D NURBS surfaces. Neocuspidizations were obtained by either shifting the upper central coaptation landmark towards the sinotubular junction or using parametric neo-landmarks placed on a centreline drawn between the centroid of the aortic root base and centroid of a circle circumscribing the 3 upper commissural landmarks.

RESULTS: The ratio of the leaflet free margin length to the geometric height was 1.83, whereas the ratio of the commissural coaptation height to the central coaptation height was 1.93. The median coaptation surface was 137 mm^2 (IQR 58) and the median load-bearing surface was 203 mm^2 (60) per leaflet. Neocuspidization multiplied the central coaptation height by 3.7 and the coaptation surfaces by 1.97 and 1.92 using the native coaptation axis and centroid coaptation axis, respectively.

CONCLUSIONS: Geometric morphometrics reliably defined the coaptation and load-bearing surfaces of aortic leaflets, enabling an experimental 3D design for the in silico neocuspidization of aortic valves.

Keywords: Aortic leaflets • Aortic root geometry • Aortic valve • 3D modelling • Computed tomography • Imaging • Three-dimensional • Ozaki procedure

ABBREVIATIONS

CC	Central coaptation
ComC	Commissural coaptation
CT	Computed tomography
gH	Geometric height
ILC	Inferior line of coaptation
LatC	Lateral coaptation
LFM	Leaflet free margin
LIL	Leaflet insertion line
MPR	Multiplanar reconstruction
NURBS	Non-Uniform Rational Basis Splines
STJ	Sinotubular junction
3D	Three-dimensional

INTRODUCTION

The physiological reliability of the aortic valve is based on its three-dimensional (3D) geometry [1–3], and whose modelling based on its geometric determinants [4, 5] could aid in the establishment of techniques for neocuspidization [6–9]. Most parts of the aortic root can be modelled through computed tomography (CT) [10]. Although aortic leaflets can be identified through multiplanar reconstruction (MPR) and volume rendering [11–15], leaflet mesh generation, based on the Hounsfield number and surface rendering, remains difficult due to insufficient spatial resolution [10].

We propose a new geometric morphometrics workflow [16] combined with Non-Uniform Rational Basis Splines (NURBS) [17, 18] to generate 3D meshes of both coaptation and load-bearing surfaces of aortic leaflets from CT [11, 12] using only their geometric determinants. Our study aimed to obtain (i) a 3D surface model of the leaflets; (ii) *in silico* aortic valve neocuspidizations [9, 19]; and (iii) a 3D solid model of the aortic valve [20] exportable for 3D printing [21], 2D flattening [7] for training purposes and ultimately patient education using 3D anaglyph visualization providing additional depth perception with stereograms [22].

MATERIALS AND METHODS

Ethics statement

The study was approved by the Assistance Publique-Hôpitaux de Marseille (RGPD/AP-HM number 2018-69) and Elsan Group (MR004-approved, 26 January 2022) Institutional Review Boards, which waived the need for individual patient consent due to the retrospective nature of the study. Contrast-enhanced CT scans of patients without heart disease were chosen based on the quality of their contrast and ECG-synchronization and reconstructed at 70–80% of the R–R interval for mid-diastole with the same slice thickness of 0.6 mm. DICOM files were imported into a viewer (Horos, version 1.1.7).

Geometric morphometrics and Non-Uniform Rational Basis Splines

Geometric morphometrics uses landmarks to increase the accuracy of 3D modelling by multiplying these points [16]. Landmarks have been defined as types I, type II, type III (referred to as semilandmarks) and can be exported with the aortic root mesh (i.e. the blood pool isosurface of the left ventricular outflow tract, sinuses and aorta) to a computer-aided design software to construct NURBS (Supplementary Material, Tables S1 and S2).

3D modelling: native aortic valve

First, a template was constructed with 4 steps:

1. The aortic root was segmented using Hounsfield threshold values [10]. Types I [top and bottom commissural coaptation (ComC) landmarks] and II (nadir of each sinus) landmarks were placed on the template (Fig. 1A) [5, 18, 20].
2. During MPR (Fig. 1B) using a bisecting centre plane orthogonal to the virtual basal ring (plane passing through the 3 nadirs) [11, 12], type I landmarks corresponding to the top and bottom central coaptation (CC) points were positioned [5]. Semilandmarks were placed along the leaflet free margins (LFMs) [12, 13] and inferior lines of coaptation (ILCs) [23]. The LFM and ILC are the superior and inferior curves of coaptation surfaces, respectively [11]. The ILC is also known as the junction line of the leaflet [1] or caudal limit of coaptation [3]. Semilandmarks were placed along the geometric height (gH) curves [2], except for the CC, passing through the corresponding nadir. The gH curves and coaptation surfaces were not always located in the same bisecting plane due to the frequent asymmetry of the leaflets [15, 24]. Additional semilandmarks in the radial directions were placed; they were not for modelling but to assess the reliability of the 3D modelling of the leaflet load-bearing surfaces.

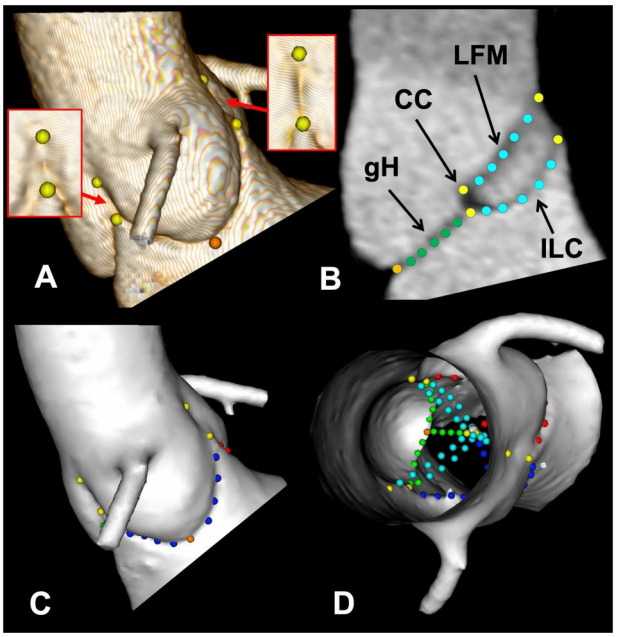

Figure 1: Geometric Morphometrics. (**A**) Volume rendering with commissural and nadir landmarks. Red arrows: commissural coaptation landmarks. (**B**) Multiplanar reconstruction with semilandmarks. (**C**) Semilandmarks on the leaflet insertion lines in surface rendering. (**D**) Complete template. CC: central coaptation; gH: geometric height; ILC: inferior line of coaptation; LFM: leaflet free margin.

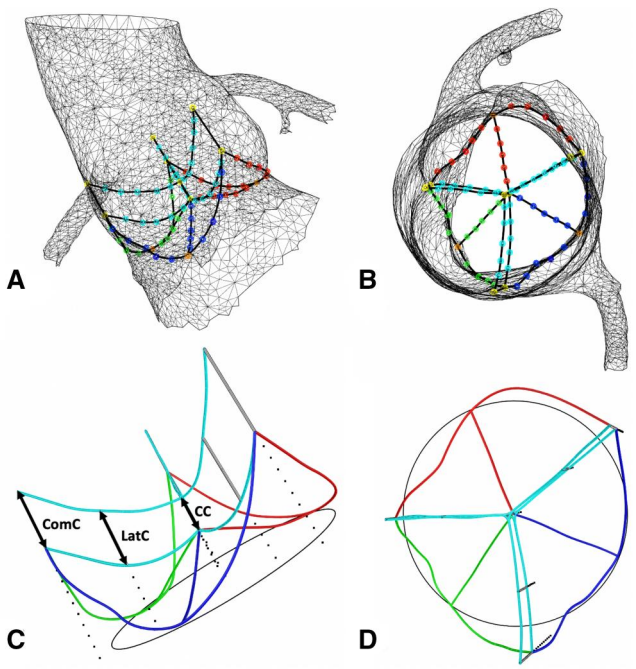

Figure 2: NURBS. (**A**, **B**) Landmarks, semilandmarks and aortic root mesh. (**C**, **D**) NURBS lines and curves. Black double-headed arrows: coaptation lines. Nadirs are not always at the middle of the leaflet insertion line. Black circle: virtual basal ring. Dotted lines: distance between the different coaptation heights and the plane of the aortic root base. CC: central coaptation; ComC: commissural coaptation; LatC: lateral coaptation.

3. Using surface rendering, semilandmarks were placed along the leaflet insertion line (LIL) on the aortic root [13], except for the ComC (Fig. 1C).
4. The template was exported as an .obj file, which included the landmarks, and aortic root as a triangle-based mesh (Fig. 1D).

Second, the files were imported into a computer-aided design software (Rhinoceros, version 7) that uses NURBS to create a 3D mathematical representation from landmarks and semilandmarks defined as control points.

1. ControlPoint NURBS curves were used to draw each geometric determinant of the leaflets, as well as the CC, lateral coaptation (LatC) [3, 17] and ComC heights [1, 5, 17, 20, 23, 25] (Fig. 2A and B). The LatC heights were measured using a line drawn between the middle of the LFM and the middle of the ILC, limited to the commissure under study (Fig. 2C and D). gH measurements included the CC height, whereas LIL measurements included the 2 ipsilateral ComC heights.
2. Coaptation and load-bearing surfaces were independently modelled from a network of NURBS curves and had been measured at this stage (Fig. 3A and B). Coaptation surfaces comprised a network of four NURBS curves (LFM, ILC and 2 ComC). Load-bearing surfaces comprised a network of 3 NURBS curves [ILC, gH and LIL (without the ipsilateral ComC)]. These 2 surfaces were merged to create a single surface for each leaflet (Fig. 3C and D).
3. NURBS surfaces of the leaflets were joined with the aortic root mesh to constitute the 3D model. After thickening the aortic root (1 mm) and leaflets (0.3 mm), the model was exported as a PLY file for 3D solid modelling and stereoscopic visualization (Fig. 4A–D).

3D modelling: neocuspidization

The principle of the Ozaki procedure is to raise the pericardial neo-LFM to the level of the sinotubular junction (STJ) [6, 7].

Using the native coaptation axis, simulating leaflet extension. From the previous models, landmarks corresponding to the LFMs were removed. The load-bearing surfaces remained unchanged.

The top CC landmark was transferred to the plane of the STJ along an extension of the CC line. The neo-LFMs were redrawn as straight lines between the top commissural landmarks and the top CC neo-landmark (Fig. 5A and B).

Using the centroids of the STJ and aortic root base. This approach was taken to simulate neocuspidization after leaflet resections. The parametric values were defined as the mean values of the previously measured aortic valves.

The new CC line connected the centroid of the STJ (centroid of a circle circumscribing the 3 upper commissural landmarks) [5] and the centroid of the aortic root base. As the shape of the aortic root base is elliptical, we used the centroid of the elliptical surface of the left ventricular outflow tract corresponding to the same plane as the virtual basal ring [26]. The height of the bottom CC neo-landmark on this central axis is parametric. Parametric heights of the bottom LatC neo-landmarks, relative to the aortic root base, were projected onto a line passing, for each commissure, through both the middle of the neo-LFM and the middle of a straight line drawn between the bottom ComC landmark and the bottom CC neo-landmark (Fig. 5C).

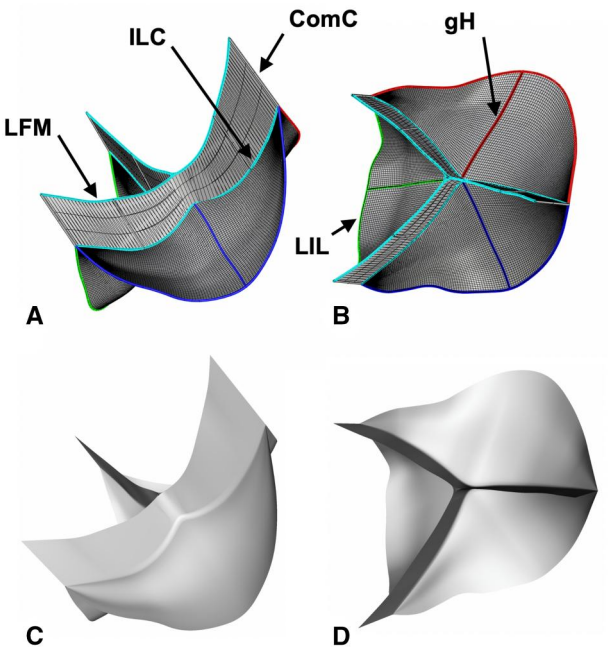

Figure 3: 3D surface modelling. (**A**, **B**) NURBS surfaces as a network of lines and curves. (**C**, **D**) Merging of coaptation and load-bearing surfaces. ComC: commissural coaptation; gH: geometric height; ILC: inferior line of coaptation; LFM: leaflet free margin; LIL: leaflet insertion line.

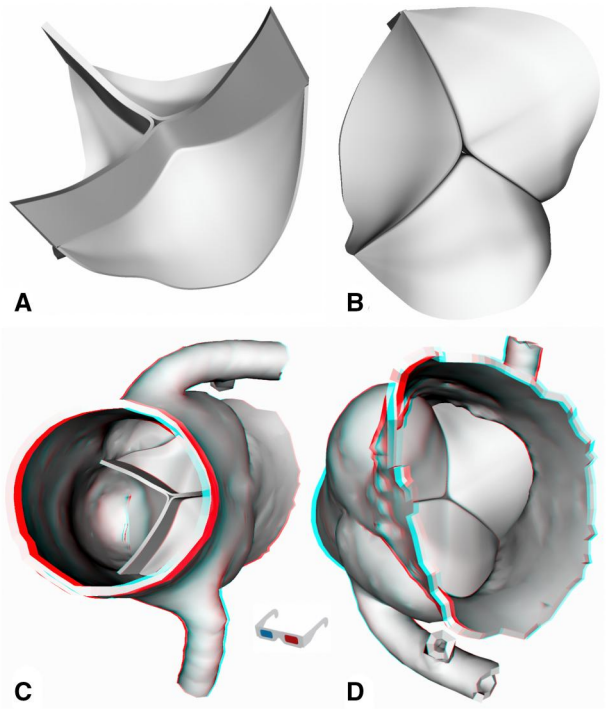

Figure 4: 3D solid modelling. (**A**, **B**) Aortic leaflets. (**C**, **D**) Aortic root using stereoscopic visualization requiring anaglyph glasses.

The bottom coaptation neo-landmarks (commissural, lateral and central) were interpolated to obtain the ILC neo-curves. The LFM neo-curves were described as polylines between the top ipsilateral commissural landmarks and the neo-landmark located at the centroid of the STJ. Neo-gH curves were modelled as straight lines between the nadir of each sinus and the bottom

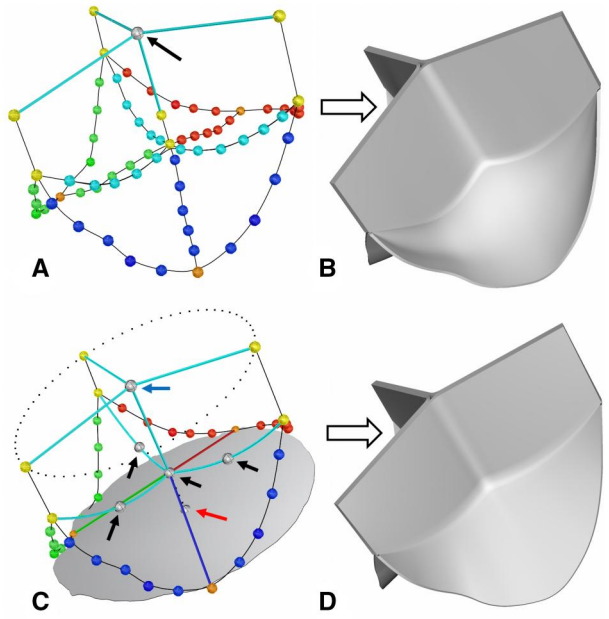

Figure 5: Neocuspidization. (**A**) Using the native coaptation axis. Black arrow: neo-landmark located at the top of the central coaptation. (**B**) Neo-leaflets with different LFM lengths. (**C**) Using the centroids axis. Black arrows: lateral and central coaptation neo-landmarks. Blue arrow: centroid of the dashed circle circumscribing the three top commissural landmarks. Red arrow: centroid of the aortic root base (grey shaded surface). Blue, red and green lines: neo-gH lines. (**D**) Neo-leaflets with identical LFM lengths. gH: geometric height; LFM: leaflet free margin.

neo-landmark of the CC given the assumption that load-bearing surfaces are curved in only 1 direction [1, 4, 23]. Surfaces were modelled as described earlier (Fig. 5D).

Statistical analysis

All variables are expressed as median (interquartile range). In addition, for each aortic valve, a single value was defined as the arithmetic mean of the values measured for a given parameter of each of the 3 leaflets, as well as for lateral and ComC data of the 3 commissures. Non-coronary leaflets, left coronary leaflets and right coronary leaflets were compared using the Kruskal–Wallis test. Comparisons between the mean ComC heights and the mean LatC heights and between mean LFMs and mean ILCs were conducted using the Wilcoxon signed-rank test. Statistical analyses were performed using Stata software (StataCorp. 2013. Stata Statistical Software: Version 13. College Station, TX: StataCorp LP).

RESULTS

We retrospectively analyzed the CT scans of 10 patients with a median age of 29 (11.8) years [(range 18–35 years); 7 men]. Measurements of NURBS are summarized in Table 1, with no significant differences having been found between measurements of the geometric determinants of the three leaflets. The median LFM/gH ratio was 1.83 (0.15). The median heights of the ComC and LatC did not differ significantly ($P = 0.17$). The median ratio of ComC to CC heights was 1.93 (0.32). The median lengths of the LFM and ILC were slightly but significantly different ($P = 0.028$).

Table 1: Aortic leaflet measurements

Variables, median (IQR)	Values ($n = 10$)	Range	P-value[a]
Native aortic valves			
Mean leaflet geometric height (mm)	17.2 (2.7)		0.17
NC	17.9 (2.4)	15.7–20.4	
RC	16 (3.3)	14.7–19.6	
LC	16.5 (3)	14.8–20.4	
Effective height (mm)	8.3 (0.6)	6.9–10.2	
Central coaptation height (mm)	3.1 (0.5)	2.3–4.5	
Mean lateral coaptation height (mm)	5.8 (0.8)		0.99
NC/LC commissure	5.5 (0.8)	4.6–8.7	
LC/RC commissure	5.7 (0.6)	4.6–7.5	
RC/NC commissure	6.6 (1.8)	5.1–8.8	
Mean commissural coaptation height (mm)	6.2 (1.7)		0.96
NC/LC commissure	6.7 (2.9)	3.2–10.1	
LC/RC commissure	7.1 (1.7)	4.3–8.4	
RC/NC commissure	6 (1.5)	5.2–10.1	
Mean leaflet insertion line (mm)	49.2 (9.8)		0.91
NC	47.7 (9.1)	40.1–56.4	
RC	48.8 (11.2)	43.1–57.4	
LC	48.7 (7.3)	40.2–56.9	
Mean leaflet free margin (mm)	31.4 (7.6)		0.21
NC	31.4 (6.8)	25.9–37.8	
RC	32 (7.7)	28.2–38.3	
LC	30.6 (6.9)	23.5–35.1	
Mean leaflet inferior line of coaptation (mm)	29 (5.2)		0.18
NC	29.1 (4.5)	26.7–36	
RC	30 (6.5)	26.9–39	
LC	27.8 (4.3)	23.9–34.4	
Mean leaflet load-bearing surface (mm^2)	203 (60)		0.63
NC	215 (58)	157–242	
RC	191 (61)	154–318	
LC	187 (67)	161–271	
Mean leaflet coaptation surface (mm^2)	137 (58)		0.15
NC	141 (62)	102–202	
RC	146 (69)	114–212	
LC	125 (49)	91–185	
Neocuspidization using the native coaptation axis			
Central coaptation height (mm)	12 (2.3)	9.4–14.4	
Mean leaflet coaptation surface (mm^2)	282 (131)		0.12
NC	286 (126)	200–375	
RC	291 (135)	214–384	
LC	260 (114)	172–340	
Neocuspidization using the centroid of aortic root base			
Central coaptation height (mm)	12.3 (3.2)	10–14.9	
Mean leaflet load-bearing surface (mm^2)	201 (58)		0.46
NC	210 (59)	159–258	
RC	190 (62)	147–274	
LC	197 (52)	158–270	
Mean leaflet coaptation surface (mm^2)	272 (134)		0.84
NC	267 (139)	186–373	
RC	281 (134)	194–387	
LC	269 (129)	176–364	

[a]Kruskal–Wallis test across all three leaflets.
IQR: interquartile range; LC: left coronary leaflet; NC: non-coronary leaflet; RC: right coronary leaflet.

Distances <1 mm were observed between each load-bearing surface of the leaflets and the corresponding additional radial semilandmarks: 0.37 (0.12) mm [range 0.18–0.53], 0.34 (0.18) mm [0.25–0.61] and 0.38 (0.22) mm [0.19–0.59], for the non-coronary, right coronary and left coronary leaflets, which were considered nonsignificant (Supplementary Material, Fig. S1).

Using successively the native and centroid coaptation axes, the median ratios of neocuspidization CC heights to native CC heights were 3.72 (0.9) and 3.76 (0.8), respectively. The median ratios of neocuspidization coaptation surfaces to native coaptation surfaces were 1.97 (0.19) and 1.92 (0.18), respectively, using the native coaptation axis and the centroid coaptation axis.

DISCUSSION

3D modelling of the native aortic valve

The ability to export landmarks with the aortic root mesh is the essential part of this workflow given that the mesh generation of aortic leaflets is usually incomplete [10], although they are discernible in MPR [11, 12]. The use of ComC heights and ILCs increase the accuracy of this 3D modelling by separately modelling coaptation and load-bearing surfaces with a physiological diastolic pressure [14]. Although the number of patients included herein was quite modest, it was a population of young

patients with no age-related abnormalities and would rarely benefit from CT.

NURBS provide free-form modelling to design parametric shapes [18], defined in the systole with the application of a pressure load to reproduce the diastole [17], or individualized shapes directly in the diastole as described in this study. This individualized 3D modelling respects the geometry of the aortic valve in terms of the elliptical shape of the aortic root base with respect to the circular aspect of the STJ [26], asymmetry of the leaflets [15, 24] and tilt of the aortic valve [27].

NURBS lines and curves. The values obtained for the geometric determinants and the LFM/gH ratio were similar to measurements reported previously [3, 4, 12, 14, 15]. Only 1 previous measurement had been reported for ComC height under physiological conditions in the diastole [1], although it is often integrated into 3D modelling and in fact not measured directly [4, 5, 18–20].

The ComC height is different from the commissural height that includes the intervalvular triangles [3, 12]. It corresponds to the parallel lines of leaflet insertion over a certain distance [4, 5, 20, 23, 25]. Swanson and Clark [1], who used silicone casts at 80 mmHg to assess the aortic valve in the closed position, found a ratio of 2.17 between ComC height and CC height, whereas our study found a ratio of 1.93. Thubrikar, citing Swanson's study, reported this value as equal to 7.1 mm [23].

NURBS surfaces. The left coronary leaflet tended to be smaller than the others, as in previously published data [3, 12, 14, 15]. The 3D load-bearing leaflet shapes were accurately reconstructed during the 3D modelling process given that the additional landmarks in radial directions were at sub-millimetre distances (Supplementary Material, Fig. S1). We believe it essential to consider the 3 coaptation heights (central, lateral and commissural) and the ILCs when modelling the coaptation surfaces and load-bearing surfaces.

Neotricuspidization of the aortic valve

Glutaraldehyde-treated autologous pericardium and native leaflets differ in their biomechanical characteristics (anisotropic and hyperelastic material properties) but, in this workflow, are both modelled in the pressurized geometry in diastole [19, 23, 28, 29].

Although the size of each neo-leaflet is defined by the intercommissural distance [6, 7], it could be desirable to define the shape of the leaflets from the preoperative imaging [6] and 3D printing [30].

We demonstrate that the Ozaki procedure almost doubles the coaptation surface of the neo-leaflets. When the central axis of coaptation is unidentifiable, the use of centroids becomes necessary:

1. For the STJ: It is preferable to use the centroid of a circle circumscribing the 3 superior commissural landmarks [31], as this allows us to obtain 3 neo-LFMs of equal length, regardless of the asymmetry of the commissural orientation of the tricuspid aortic valve. In addition, different centres could be used: (i) the centroid of a triangle defined by the 3 commissures [27], (ii) the Torricelli point to obtain 3 leaflets of the same angular sector [9] and (iii) the centroid of the plane corresponding to the STJ [32].
2. For the aortic root base: using the centroid of the surface allows us to consider its elliptical shape [26]. Another way would be to use the centroid of the deepest point of each intervalvular triangles [27], or the centroid of 'sinus boundaries' [33], which however does not incorporate the different heights of coaptation and does not allow the angle of the leaflet free edge (ϕ) to be modelled [23].

Applications of 3D surface modelling

3D solid modelling is the gateway to several applications for training and teaching purposes. Inexpensive anaglyph stereoscopic visualization improves depth perception and could contribute to patient education (Figs 4C and D and 6) [22].

3D printing. The 3D printing of the aortic leaflets (Fig. 6A) can be used to obtain pericardial leaflets in 3D or 2D projection (Fig. 6B and C). These neo-leaflets could be used for the training, simulation and teaching of the Ozaki procedure, including its experimental insertion into a 3D-printed aortic root [6, 21].

2D Surface flattening of the aortic leaflets. The leaflets include a developable surface with curvature in only 1 direction (coaptation surface) and an essentially non-developable surface (load-bearing) when using curvature analysis of our models. Although the load-bearing surfaces are generally considered developable [1, 23], they are often too complex to flatten into 2D patterns. The 2D projection of an entire merged leaflet (a complex double-curved surface) cannot be performed, except possibly using transverse lines [26]. As stated by Swanson and Clark, 'The leaflet is developable onto a plane with a cut required along part of the junction line between the initially cylindrical part and the plane coapting surfaces' [1].

Thus, we propose a 2D projection through the following steps (Fig. 6D–F):

1. The coaptation surfaces are flattened into 2D.
2. The load-bearing surfaces are modelled in the same 2D plane as that for the coaptation surfaces by extending them using NURBS lines whose length is equal to gH for the median axis and corresponds laterally to the 2 radial supplementary axes. An interpolated neo-LIL curve is then modelled with the bottom commissural landmarks and those located at the ends of these 3 extensions. These 2D load-bearing neo-surfaces are constructed as a network of neo-ILC, neo-LIL and neo-gH curves.
3. These 2 surfaces are merged and could be used as an experimental template for training neocuspidizations. Length variations in the radial or circumferential directions could be used to: (i) test different configurations of leaflet hyperelasticity and anisotropy [19], (ii) examine dimensional variations of the neo-leaflet from the physiologically loaded (CT) state to the unpressurized state (application of the template onto the autologous pericardium) [28] and (iii) adapt the modelling to prevent CC failure [2].

Limitations

First, the dimensions obtained during the modelling process may vary depending on: (i) the Hounsfield density of the blood volume, which may vary depending on the centre's injection protocol, and (ii) the level/width applied to the greyscale

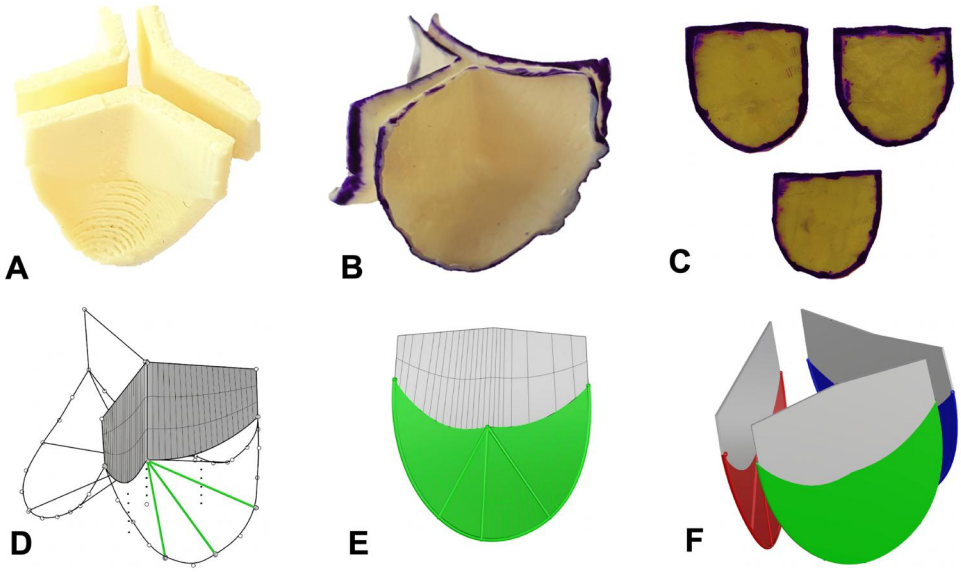

Figure 6: Neocuspidizations using the native coaptation axis. (**A**) 3D printing. (**B**) 3D moulding and (**C**) 2D flattening of the heterologous pericardium (excluding the margin 'W' to suture, and the geometric corrections 'α' and 'β' as described par S. Ozaki [7]). The pericardium is treated with glutaraldehyde after (**B**) or before (**C**) application on the 3D printed template. (**D**) The 3D template with the gH and radial additional axes (green lines). (**E**) 2D flattening of the coaptation surface merged with the neo-leaflet load-bearing 2D surface. (**F**) 2D solid modelling of the 3 neo-leaflets. gH, geometric height.

histogram of the DICOM viewer [10, 12–14]. To avoid these distortions, the pixel value was kept constant during modelling [10].

Second, the spatial resolution of CT is suboptimal. Nonetheless, ComC heights and ILCs were clearly identifiable, as were other geometric determinants in MPR. However, CT measurements will need to be compared with echocardiographic data to combine the spatial resolution of CT [10, 12] with the temporal resolution of echocardiography [5].

Third, the duration of the workflow (1.5 h) may seem excessive; however, semi-automated procedures are being developed [33], and segmentation can be fully automated if the synchronization and contrast of the CT are of good quality [10, 12].

Fourth, structural anomalies (fenestrations, etc.) and bicuspid valves have yet to be considered. Nevertheless, the measurement of LFM and gH can be performed for pathological valves and could help determine the repair strategy and length of LFM plication [3].

Finally, the height of the neo-leaflets and resulting risk of coronary perfusion should also be considered [33]. Therefore, the clinical relevance of this 3D workflow, including for the geometry and systolic dynamics of the coaptation surfaces, will need to be studied *in silico*, to determine the fluid–structure interaction, and *in vitro* before any clinical use [19].

CONCLUSION

Geometric morphometrics, applied to the geometric determinants, enables the 3D shape of the aortic leaflets to be precisely defined. Separate modelling of the coaptation and load-bearing surfaces, through the additional use of ComC heights and ILCs, provides a surface 2D planar projection of the neo-leaflets that allows for the in silico experimental study of aortic neocuspidizations.

These 3D models could facilitate surgical training or make surgical neocuspidizations more intuitive for patient teaching, whether through 3D printing or stereoscopic anaglyph visualization.

SUPPLEMENTARY MATERIAL

Supplementary material is available at *ICVTS* online.

ACKNOWLEDGEMENTS

The authors thank Mr Vincent Long, from the LMA, for the 3D printing of the aortic valve.

FUNDING

The authors received no funds for this study.

Conflict of interest: none declared.

DATA AVAILABILITY

Data are available on request, with the exception of STL files for ethical reasons.

Author contributions

Loïc Georges Macé: Conceptualization; Data curation; Methodology; Software; Writing—original draft; Writing—review and editing. **Tom Fringand:** Conceptualization; Methodology; Software; Writing—review and editing. **Isabelle Cheylan:** Methodology; Software; Writing—review and editing. **Laurent Sabatier:** Resources; Validation; Writing—review and editing. **Laurent Meille:** Resources; Validation; Writing—review and editing. **Marien Lenoir:** Formal analysis; Methodology; Writing—review and editing. **Julien Favier:** Conceptualization; Methodology; Software; Supervision; Writing—review and editing.

Reviewer information

Interactive CardioVascular and Thoracic Surgery thanks Samuel Heuts and the other anonymous reviewers for their contribution to the peer review process of this article.

REFERENCES

[1] Swanson WM, Clark RE. Dimensions and geometric relationships of the human aortic valve as a function of pressure. Circ Res 1974;35:871–82.

[2] Bierbach BO, Aicher D, Issa OA *et al.* Aortic root and cusp configuration determine aortic valve function. Eur J Cardiothorac Surg 2010;38:400–6.

[3] De Kerchove L, Momeni M, Aphram G *et al.* Free margin length and coaptation surface area in normal tricuspid aortic valve: an anatomical study. Eur J Cardiothorac Surg 2018;53:1040–8.

[4] Labrosse MR, Beller CJ, Robicsek F, Thubrikar MJ. Geometric modeling of functional trileaflet aortic valves: development and clinical applications. J Biomech 2006;39:2665–72.

[5] Labrosse MR, Beller CJ, Boodhwani M, Hudson C, Sohmer B. Subject-specific finite-element modeling of normal aortic valve biomechanics from 3D+t TEE images. Med Image Anal 2015;20:162–72.

[6] Ozaki S, Kawase I, Yamashita H, Uchida S, Takatoh M, Kiyohara N. Midterm outcomes after aortic valve neocuspidization with glutaraldehyde-treated autologous pericardium. J Thorac Cardiovasc Surg 2018;155:2379–87.

[7] Ozaki S, inventor. Japanese Organization for Medical Device Development, Inc, assignee. USPatent 9,788,940 B2. 17 October 2017. https://patents.google.com/patent/US20160317297 (28 January 2023, date last accessed).

[8] Mourad F, Shehada S-E, Lubarski J *et al.* Aortic valve construction using pericardial tissue: short-term single-centre outcomes. Interact CardioVasc Thorac Surg 2019;28:183–90.

[9] Todurov B, Mokryk I, Batsak B, Ponych N. Computed tomography-guided aortic valve neocuspidization; details of preoperative assessment and surgical technique. Interdiscip Cardiovasc Thorac Surg 2023; https://doi.org/10.1093/icvts/ivac290.

[10] Hosny A, Dilley JD, Kelil T *et al.* Pre-procedural fit-testing of TAVR valves using parametric modeling and 3D printing. J Cardiovasc Comput Tomogr 2019;13:21–30.

[11] Toh H, Mori S, Tretter JT *et al.* Living anatomy of the ventricular myocardial crescents supporting the coronary aortic sinuses. Semin Thorac Cardiovasc Surg 2020;32:230–41.

[12] Tretter JT, Izawa Y, Spicer DE *et al.* Understanding the aortic root using computed tomographic assessment: a potential pathway to improved customized surgical repair. Circ Cardiovasc Imaging 2021;14:1056–74.

[13] Kamiya K, Nagatani Y, Matsubayashi Y *et al.* A virtual-reality imaging analysis of the dynamic aortic root anatomy. Ann Thorac Surg 2021;112:2077–83.

[14] Jelenc M, Jelenc B, Poglajen G, Lakič N. Aortic valve leaflet and root dimensions in normal tricuspid aortic valves: a computed tomography study. J Card Surg 2022;37:2350–7.

[15] Yang DH, Kim D-H, Handschumacher MD *et al. In vivo* assessment of aortic root geometry in normal controls using 3D analysis of computed tomography. Eur Heart J Cardiovasc Imaging 2017;18:780–6.

[16] Bardua C, Felice RN, Watanabe A, Fabre A-C, Goswami A. A practical guide to sliding and surface semilandmarks in morphometric analyses. Integr Org Biol 2019;1:obz016.

[17] Morganti S, Auricchio F, Benson DJ *et al.* Patient-specific isogeometric structural analysis of aortic valve closure. Comput Methods Appl Mech Engrg 2015;284:508–20.

[18] Xu F, Morganti S, Zakerzadeh R *et al.* A framework for designing patient-specific bioprosthetic heart valves using immersogeometric fluid–structure interaction analysis. Int J Numer Method Biomed Eng 2018;34:e2938.

[19] Hammer PE, Chen PC, del Nido PJ, Howe HD. Computational model of aortic valve surgical repair using grafted pericardium. J Biomech 2012;45:1199–204.

[20] Dallard J, Boodhwani M, Labrosse MR. Aortic valve mechanics. In: Labrosse MR (ed). Cardiovascular Mechanics. Boca Raton, FL: CRC Press / Taylor & Francis Group, 2018, 280–312.

[21] Russo M, Koenigshofer M, Stoiber M *et al.* Advanced three-dimensionally engineered simulation model for aortic valve and proximal aorta procedures. Interact CardioVasc Thorac Surg 2020;30:887–95.

[22] Izawa Y, Nishii T, Mori S. Stereogram of the living heart, lung, and adjacent structures. Tomography 2022;8:824–41.

[23] Thubrikar M. The Aortic Valve. New York, London: Informa Healthcare, 2011 (online 2017), 11–30.

[24] Becker AE. Surgical and pathological anatomy of the aortic valve and root. Oper Tech Cardiac Thorac Surg 1996;1:3–14.

[25] Kunzelman KS, Grande J, David TE, Cochran RP, Verrier ED. Aortic root and valve relationships. Impact on surgical repair. J Thorac Cardiovasc Surg 1994;107:162–70.

[26] Rankin JS, Bone MC, Fries PM, Aicher D, Schäfers HJ, Crooke PS. A refined hemispheric model of normal human aortic valve and root geometry. J Thorac Cardiovasc Surg 2013;146:103–8.

[27] Berdajs D, Mosbahi S, Forro Z *et al.* Numerical analysis of the 3-dimensional aortic root morphology during the cardiac cycle. Eur J Cardiothorac Surg 2016;49:1213–21.

[28] Labrosse MR, Lobo K, Beller CJ. Structural analysis of the natural aortic valve in dynamics: from unpressurized to physiologically loaded. J Biomech 2010;43:1916–22.

[29] Yamashita H, Ozaki S, Iwasaki K, Kawase I, Nozawa Y, Umezu M. Tensile strength of human pericardium treated with glutaraldehyde. Ann Thorac Cardiovasc Surg 2012;18:434–7.

[30] Pirola S, Mastroiacovo G, Mostardini G *et al.* Preoperative Ozaki technique measures on tridimensional engineered root. J Cardiovasc Comput Tomogr 2022;16:51–3.

[31] Jelenc M, Jelenc B, Habjan S *et al.* Segmental analysis of aortic basal ring dimensions in normal and dilated tricuspid aortic roots. Interdiscip Cardiovasc Thorac Surg 2024. https://doi.org/10.1093/icvts/ivae029.

[32] Youssefi P, Gomez A, He T *et al.* Patient-specific computational fluid dynamics-assessment of aortic hemodynamics in a spectrum of aortic valve pathologies. J Thorac Cardiovasc Surg 2017;153:8–20.

[33] Lior D, Puelz C, Edwards C *et al.* Semi-automated construction of patient-specific aortic valves from computed tomography images. Ann Biomed Eng 2023;51:189–99.